

## Electron capture from H<sub>2</sub> to highly charged Th and Xe ions trapped at center-of-mass energies near 6 eV

G. Weinberg,<sup>1,\*</sup> B. R. Beck,<sup>2</sup> J. Steiger,<sup>2</sup> D. A. Church,<sup>1</sup> J. McDonald,<sup>2</sup> and D. Schneider<sup>2</sup>

<sup>1</sup>Physics Department, Texas A&M University, College Station, Texas 77843-4242

<sup>2</sup>Lawrence Livermore National Laboratory, P.O. Box 808, Livermore, California 94550

(Received 19 May 1997)

Ions with charge states as high as 80+, produced in the Lawrence Livermore National Laboratory electron beam ion trap were extracted and transferred to a Penning ion trap (RETRAP). RETRAP was operated at cryogenic temperature in the field of a superconducting magnet. The stored low-energy ions collided occasionally with H<sub>2</sub> molecules in the ultrahigh-vacuum environment of the trap, capturing one or two electrons and reducing the charge state of the ions. The number of ions was monitored nondestructively by ramping the axial oscillation frequencies of the ions through resonance with a tuned circuit composed in part of trap capacitance and an external inductor. This produced resonance signals whose square is proportional to the number of ions in each charge state. These signals were recorded vs storage time to determine the electron-capture rates. From these rates the relative electron-capture cross sections were obtained using estimates of the mean ion energies based on modeling the ion storage, and with the aid of a density calibration measurement using Ar<sup>11+</sup>. The measured total electron-capture cross sections are consistent with a linear increase with charge state  $q$ . The cross-section data for the highest charge states lie above the predictions of the absorbing sphere model, but agree within uncertainties in both experiment and theory. The true double-capture cross-section fraction for  $q > 35$  is near 25%. The results are discussed with relation to measurements on lower charge states, and with theory. [S1050-2947(98)06406-3]

PACS number(s): 34.70.+e, 39.90.+d, 34.10.+x

### I. INTRODUCTION

High charge-state and low-energy electron-transfer collisions are important in laboratory plasmas and ion sources, in astrophysical plasmas, and in certain types of potential x-ray lasers. General considerations important to the theory of these collisions are the scaling of the total cross section with ion charge state [1], the velocity dependences of the cross section in different energy regions [2], and the relationship of single-to-multiple electron capture [3]. Particular interest has focused on true double capture [4–6], in which both captured electrons remain on the ion after the collision.

At the low energies of interest here, theory has been most successful with few-electron atomic targets, particularly atomic hydrogen, but also H<sub>2</sub> and He. At these energies, the collision can often be treated as the temporary formation of a quasimolecule, with molecular wave functions and potential energies calculated as a function of the internuclear separation  $R$  of the ion and neutral target. An electron is transferred at certain avoided crossings of these potential energy curves [7]. Collisions of various ions in low charge states with H and H<sub>2</sub> have been measured and calculated over a range of energies [8–11].

At these energies, and for low charge states, this detailed quasimolecular theoretical treatment is appropriate, with calculations of orbitals for each collision pair required. The magnitudes of the capture cross sections can vary appreciably with energy and charge. Electron capture to ions with

high charge state  $q$  is expected to occur into closely spaced, highly excited states (high- $n$  states), under conditions where there are a large number of avoided crossings. The absorbing sphere model of Olson and Salop [1], based on Landau-Zener theory, applies under these conditions, while over-barrier models [12–14] apply at these and still higher energies. An important prediction of these theories is an approximately linear dependence of the total electron-capture cross section on charge state  $q$ , in contrast to an earlier prediction [15].

The lower end of the energy range for validity of the classical over-barrier model [14] for electron transfer begins near the energy of the present measurement. This static model allows calculation of the cross section for the initial populations of charge states, but not subsequent autoionization as could occur with multielectron targets. Nevertheless, it should be valid for the total capture cross section. In a collision the Coulomb barrier separating target electrons from projectile (ion) electrons ceases to be effective at some internuclear radius  $R_t^i$  which depends on the ionization energy  $I_i$  of each target atom electron. If  $R_t^i > R_{tp}$ , the distance of closest approach, then electron  $t$  becomes “molecular” and can be transferred back and forth between target and projectile. An individual “molecular” electron may end up either on the projectile or the target as the internuclear distance increases, with a probability depending on the amount of phase space available for motion around each binding center. Niehaus [14] showed that the “geometrical” cross section  $\pi(R_t^i)^2$  is the sum over all charge-changing cross sections given by this model, where  $R_1^i$  denotes  $R_t^i$  for the first electron transferred. For Th<sup>80+</sup> colliding with H<sub>2</sub>,  $R_1^i = 33.4$  a.u., and  $\pi(R_1^i)^2 \approx 10^{-13}$  cm<sup>2</sup> in reasonable agree-

\*Present address: Research, 2201 Third Street, San Francisco, CA 94107.

ment with the data presented below.

A complication with multielectron targets is multiple-electron capture, either sequentially or in a single event. Experimental studies [4] at low energy for  $q < 8$  indicated that the cross section for two-electron transfer and for single-electron transfer depended similarly on energy and charge. Multiple-electron capture into autoionizing states may occur, resulting in emission of electrons to the continuum. For example, capture of two electrons with autoionization of one may appear experimentally as single capture. The probability of an Auger process of this type is largely independent of ion charge  $q$ , since it depends only on the correlation of two captured electrons, while radiative stabilization probability scales as  $q^4$  for  $\Delta n \neq 0$  transitions. Both processes depend on the principal quantum number  $n$  of the states initially populated by the capture, which also depend on  $q$ . Nevertheless, the ratio of the Auger to radiative rates tends to scale as  $q^{-4}$ , indicating that radiative stabilization should dominate for  $q > 10$ , according to an early analysis [16]. Recent data for Xe $^{q+}$ -He collisions ( $15 < q < 42$ ) [6] show that true double capture (radiative stabilization) increases rapidly for  $q > 28$  to a plateau for  $35 < q < 42$ . This indicates that a more detailed analysis of the true double-capture rate, possibly depending on the details of ion structure, is required, and that data for still higher charge states are desirable.

The present measurements were carried out using ions with an unprecedented combination of high charge states ( $35 \leq q \leq 80$ ) and low energy (6 eV in the center-of-mass frame). These ions were produced [17] and then extracted [18] from the electron beam ion trap (EBIT) at Lawrence Livermore National Laboratory (LLNL). Some of the extracted ions were then transported to and injected into RETRAP, a cryogenic Penning ion trap located in a superconducting solenoid [19]. In RETRAP, nondestructive monitoring of signals whose squares are proportional to ion number and energy in each charge state permitted a study of the time evolution of the confined ion charges. Charge states changed when the ions collided with H<sub>2</sub> molecules existing at low density in the trap region. Following capture, the reduced-charge heavy product ions remained confined, providing information on the product ion charge states and time development, and capture rates for a string of charge states [20,21]. Measurements of the charge-exchange rates for electron capture from H<sub>2</sub> to Ar $^{11+}$  were performed. These rates combined with independent measurements of the total cross section for electron capture from H<sub>2</sub> to Ar $^{11+}$  [11,22] were used to determine  $n$ . An estimate of the mean ion energy was used to convert the reaction rates obtained from the ion storage time constants to mean total cross sections, which are compared to theoretical predictions. The total cross sections are found to increase in proportion to the charge state. True double-capture cross sections are found to be about 25% of the total, even for Th $^{80+}$ .

In Sec. II the apparatus and procedures specific to these measurements are described. The results and data analysis are presented in Sec. III. The relations of the results to current theory are discussed in Sec. IV.

## II. APPARATUS AND PROCEDURE

### A. Ion capture

The production of highly charged ions in EBIT [17], the extraction of ions from EBIT [18], and the fast extraction of

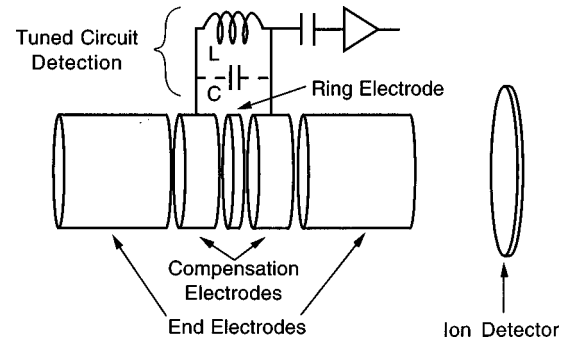


FIG. 1. Schematic diagram of the measurement system showing the ion trap and detection tuned circuit with preamplifier, and the separate particle detector.

ions followed by transport and recapture into RETRAP [19] have already been documented. The present focus is on the storage properties and detection of the ions in RETRAP for the purpose of the present electron-capture measurements. Briefly, highly charged ions of a particular element in a small range of charge states were produced by sequential electron impact ionization in EBIT [23]. After production, they were ejected from EBIT by a fast linear ramp of the potential on the center drift tube. These ions were then extracted along the magnetic field lines at a potential near 4.5 kV. A particular charge state  $q$  was selected from the extracted ion pulse by use of an analyzing electromagnet. These ions were transported electrostatically to RETRAP where they were slowed to a low kinetic energy upon entering a “deceleration tube” situated in the fringe field of the axial magnetic field of the Penning trap. The potential of this tube, which was near the EBIT extraction potential, was then rapidly pulsed lower by nearly the extraction potential, permitting those ions within the tube to emerge with energies  $< 50 q$  eV. After the slowed ions entered the Penning trap through the upper end electrode, the potential of this electrode was rapidly pulsed. This pulse, from 0 to about 90 V, was delayed, relative to the deceleration tube pulse by an amount which optimized the capture of ions. Voltages and relative time delays were all separately scanned to optimize ion capture, as evidenced by the delayed ejection of ions confined in the trap onto a particle detector mounted below the trap. The number of ions captured into the trap was limited by the number of ions delivered to RETRAP in a spatially short pulse, by the fraction of ions in this pulse within the deceleration tube when it was pulsed, and by the fraction of those ions captured into the Penning trap. For ions like Xe $^{44+}$ , an average of about 20 ions per pulse were caught, while somewhat fewer were typically trapped for Th $^{80+}$ .

### B. Ion confinement

The Penning ion trap for these measurements was of the open cylinder design described by Gabrielse, Haarsma, and Rolston [24], see Fig. 1. This trap consists of five cylindrical electrodes with radius  $\rho$ : a ring electrode, two compensation electrodes, and two end electrodes separated by  $2z_0$  (see Fig. 3 of Ref. [19]). The electrodes were chosen with a length-to-diameter ratio to produce a harmonic axial dc potential in the central region, if potentials applied to the end, compensation,

and ring electrodes had the values  $V$ ,  $0.118V$ , and  $0$ . To good approximation, this potential has the form

$$\Phi(r,z) = (C_2 V / 2d^2)(r^2/2 - z^2) \quad (1)$$

for  $r$  and  $z$  small compared to  $d$ . Here  $d^2 = (z_0^2 + \rho^2/2)/2$  and the constant  $C_2 = 0.5449$ . In this potential an ion oscillates with an axial angular frequency

$$\omega_z = (q e V C_2 / m d^2)^{1/2}. \quad (2)$$

The confining dc potential also extends inside the end electrodes, where it gradually loses its harmonic character and approaches a limiting value. This extended axial potential falls below a purely harmonic potential, so confined ions with the same mass-to-charge ratio  $m/q$ , oscillating axially with large amplitudes, have a lower frequency than those oscillating with lower amplitude in the harmonic region. Thus the width and shape of the measured axial resonance provided information on the axial energy distribution for the stored ions.

The uniform axial magnetic field  $B$ , required to inhibit radial loss of the ions, was produced by a superconducting Helmholtz pair of coils. It was operated near 4 T for the present measurements. The Penning trap, plus a tuned circuit and preamplifier described below, were situated at 4.2 K in the cold bore of this cryogenic system.

The voltages of the end electrodes of the trap were rapidly (tens of ns) pulsed from (or to) zero potential to capture (or release) the ions. To ensure voltage stability and reduce electrical noise, the fast pulsers were connected to the trap by relays in parallel with 1 M $\Omega$  resistors. The relays were closed during pulsing, and opened otherwise. A low ramp voltage was additionally applied to the end electrodes during ion detection to sweep the axial frequencies of the ions. Other low-amplitude wave forms were also employed for specific purposes (see below).

### C. Ion detection

A low-capacitance high- $Q$  tuned circuit was constructed by attaching the trap compensation electrodes to a 770  $\mu$ H inductor formed by winding a single layer of copper wire onto a ceramic form. This inductance tuned out the capacitance of the trap, plus stray capacitance, at a resonant frequency  $\omega_0/2\pi = 1.21$  MHz, with a quality factor  $Q$  near 250 at low temperature. This  $Q$  provided good signal-to-noise ratios, and an appropriate bandwidth. A low-temperature broadband GaAs preamplifier similar to one discussed in Ref. [25], with high input impedance and low output impedance, amplified the voltage signal appearing across the tuned circuit by a factor of 3. A broadband low-noise room-temperature amplifier further amplified the signal, which was filtered and detected in a 9 kHz bandwidth by a spectrum analyzer operated in the “zero-span” mode. The time sweep of the spectrum analyzer was synchronized with the voltage ramp of the trap end electrodes. The trap voltage  $V$  was initially set so that the frequency of the ion charge state injected into the trap was below the tuned-circuit resonance. Voltage signals were detected on the tuned circuit as the ions were swept through resonance. Resonance of the axial oscillation frequency of the injected charge state with the tuned-

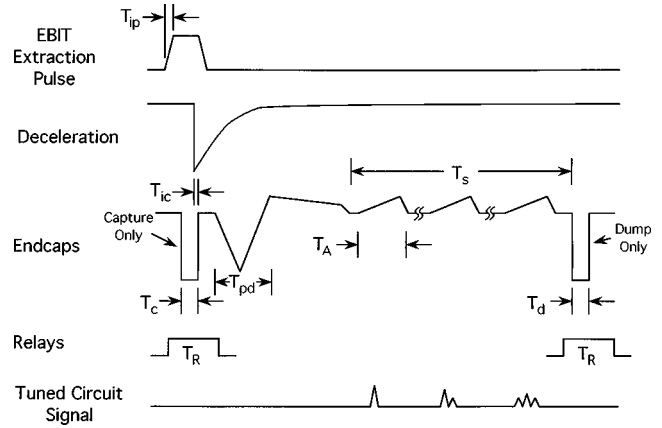


FIG. 2. The timing pattern and wave forms used in the measurements are diagrammed. Initially the ions are captured into the trap by the deceleration pulse plus a short downward pulse of the potential on the top end electrode. The ions are then stored and detected, and are finally dumped by a short downward pulse of the potential on the bottom end electrode. The typical values of the labeled time intervals are  $T_{ip} = 20 \mu\text{s}$ ,  $T_c = T_d = 20 \mu\text{s}$ ,  $T_{ic} \approx 2 \mu\text{s}$ ,  $T_{pd} = 1 \text{ s}$ ,  $T_A = 1 \text{ s}$ . The detection sweeps were repeated 20 times during the storage interval (the first two and last one are diagrammed). For Th the interval between detection sweeps was 5 s, making  $T_s = 102 \text{ s}$ . Longer times for Xe and Be were used. The relay pulse times  $T_R$  were not critical. The deceleration voltage edge was about 10 ns in duration. Representative signals obtained during the three diagrammed sweeps are indicated.

circuit frequency occurred at a low value of the ramp voltage. Any lower charge state then appeared as a signal at a higher value of the ramp voltage. One sees that the product  $q_i V$  must be constant for a fixed value of  $\omega_z$ , so for small decrements in charge the voltage ramp is equivalent to a linear charge scale. The wave form variations and timing cycle are diagrammed in Fig. 2.

The mean squared voltage signal induced by  $N_i$  ions with mean axial energy  $E_z$  is given by the expression

$$\overline{V_i^2} = N_i R E_z / \tau_z = N_i E_z (q e \gamma)^2 R^2 / 4 m d^2, \quad (3)$$

where  $R = Q / \omega_0 C$  was the resistance of the tuned circuit at resonance, and  $\tau_z = 4 m d^2 / q^2 e^2 \gamma^2 R$  was the one-dimensional damping time constant for the axial energy of ions when held at tuned-circuit resonance. The coupling factor  $\gamma$  for the compensation electrodes was calculated to be 0.9 [24]. The total mean squared voltage signal across the tuned circuit was the sum of  $V_i^2$  and  $V_n^2$ , where  $V_n^2$  was the quadrature sum of the residual Johnson noise of the tuned circuit at resonance plus contributions from the first preamplifier. Representative individual and cycle-averaged squared signals appear in Figs. 3 and 4, respectively.

As discussed in Sec. II B, higher-energy ions oscillate in a less harmonic potential. When individual ions with the same charge were detected, narrow resonance peaks such as those shown in Fig. 3 would appear. However, the position of the peaks on the ramp could shift significantly relative to the linewidth, due to an ion in one measurement having higher energy than a different ion in another measurement. When many ions were trapped, and the squared signals averaged, broadened peaks with limited charge-state resolution were

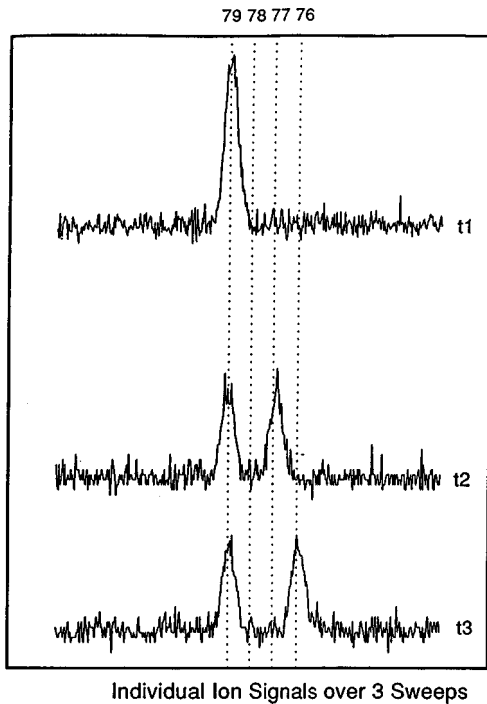


FIG. 3. The peak at measurement time  $t_1$  is due to two Th ions, initially in charge state  $q = 79$ , nondestructively detected. At time  $t_2$  the charge state of one ion has decreased due to capture of two electrons in one or two collisions with H<sub>2</sub> during the interval between measurements, resulting in two single-ion peaks in different charge states. The other ion captures no electrons up to time  $t_3$  in this measurement. The signal is a voltage with arbitrary magnitude, which depends on the amplification.

observed, as shown in Fig. 4(b). To improve the resolution of these peaks, the trap voltage  $V$  was temporarily reduced adiabatically by a factor of up to 6, after ions were confined, but before the electron-capture measurement. This “pre-

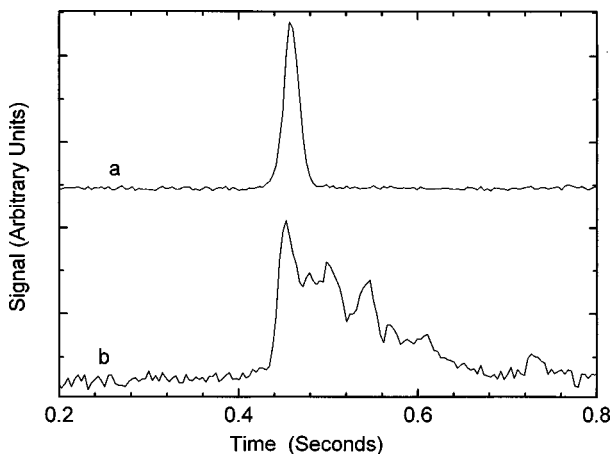


FIG. 4. (a) The squared signal of Xe<sup>44+</sup> ions recorded just after the “pre-dump” phase, used to remove the highest-energy ions from the trap. The data were averaged over many cycles to reduce the noise. (b) A similar cycle-averaged, squared signal for Xe<sup>44+</sup> ions, but with the full range of energies initially found for ions captured into the trap. The structure is due to some energies being more probable than others for higher-energy ions oscillating anharmonically. The anharmonic oscillation broadens the signal, by contributing lower-frequency signal strength.

dump” resulted in the loss of the highest-energy ions over the axial potential well barriers. For Xe ion measurements with low collision rates (lower operating pressure), the trap voltage was then slowly (several seconds) ramped from slightly above resonance to slightly below resonance, in order to resistively cool the remaining ions by energy loss to the tuned circuit. Following the predump or both preparatory procedures, the ions were detected using the voltage ramp. The peaks then had significantly narrower widths for improved charge-state resolution [Fig. 4(a)].

#### D. Measurement and analysis procedure

The data were accumulated and analyzed in two different ways. All measurements were of voltage signals on the tuned circuit, produced by ramping the axial oscillation frequencies of the ions through resonance. Each sweep of the spectrum analyzer was recorded for all collected data. In some measurements an individual ion was captured and monitored as a function of time by periodically ramping its oscillation frequency through the tuned-circuit resonance. After an electron-capture collision, the heavy product ion remained confined in the trap. Because each measurement was recorded and stored, the time history of the charge states of individual ions could be followed [26]. Since the squared signal is proportional to axial energy [Eq. (3)], and since the ion axial energy decreases due to damping during each ramp through resonance, the signal decreased slowly with measurement time even if the charge did not change during typically 20 measurement sweeps. This form of data analysis, which was basically digital in nature, was not affected by the changes in axial energy. Figure 3 shows the time development of the signals due to two simultaneously confined Th ions, both initially with  $q = 79+$ . At each measurement, the charge state of each ion was determined, and from several histories like this, the mean collision rate with H<sub>2</sub> molecules. It was found that the histories of at most three ions per measurement could be unambiguously followed in this way. The data for several charge states of individual ions were accumulated over a number of histories to obtain the total transfer rate and the ratio of the true double-to-total electron-capture cross section.

The second measurement technique was based on averaging the analog data at each delay time from many separate measurement cycles. Otherwise, the same apparatus and techniques were employed. This second technique was used for all of the data. The analog data were analyzed to determine the area under the squared voltage signal for each charge state. These areas were determined either by integrating between ramp-voltage limits, or by fitting the data peaks. Both methods were found to give comparable results, when compared for particular measurement parameters. These areas were proportional to the ion number  $N$ ,  $q^2$ , and the mean axial energy  $E_z$ , at each time according to Eq. (3).

The initial ion axial energy (of the sample surviving the preparation) was analyzed using observed signal widths together with calculations of the expected anharmonic frequency shifts as a function of oscillation amplitude in the trap potential. Based on this analysis, the average axial ion energy at the start of the measurements was  $4q$  eV in the laboratory frame, or approximately 2.6 eV in the center-of-

mass frame. These estimates were also in accord with signal amplitudes measured for single ions. Energy also resided in the cyclotron motion of the ions (see below).

In determining the relative ion number from analog signals there is a correction to the signal related to the charge. The squared signal dependence is explicitly proportional to  $q^2$  for ions with a constant axial amplitude of oscillation. However, the detection sweep is adiabatic, so the axial component of the action is a constant of the motion during the ramp, but not the axial energy. The well depth for lower-charged ions is increased more before detection. Considering the variation of the squared signal due to the changes in charge and mean axial energy, a  $q^{3/2}$  dependence results, requiring a small charge-state correction to the data.

Corrections to the raw data for other changes in the mean axial ion energy with ion storage time were also required. These changes are described and discussed separately, before the general analysis procedure is presented below. Changes in the mean axial energy occurred in part due to the small energy loss during measurement as noted above. This loss was determined using the fitted value of the cooling time constant obtained in the measurements (see below). It was compatible with the calculated time that the ions were in resonance with the tuned circuit during the measurement cycle. This energy loss associated with detection was also experimentally determined by measuring the loss while using different numbers of detection sweeps in short intervals on otherwise identical measurements. Results similar to the calculations were obtained.

It was also noted that despite these straightforward corrections for charge state and energy, the sum of all of the numbers of highly charged ions tended to change with measurement time instead of remaining constant. This could be a consequence of product ion loss, or to additional changes in the mean axial ion energy during the course of a measurement, or to instrumental effects. No heavy product ion loss from the trap due to collisions was observed in the few-ion digital analysis. This is expected, since the energy contributed to the highly charged heavy ion in the breakup of the quasimolecule following electron transfer is negligible compared to ion confinement energies in the present measurements. Low-charge ions such as  $\text{Be}^+$  and  $\text{Be}^{2+}$ , which were captured into the trap in numbers up to  $10^5$  from a pulse of ions produced by a metal vapor vacuum arc (MEVVA) source mounted above the trap, had storage times exceeding 4000 s (including charge changing due to electron capture), demonstrating that ion loss due to radial diffusion, for example, was negligible during the much shorter time-scale measurements on the highly charged ions.

However, there can be significant energy transfer between the axial and radial degrees of freedom of the confined ion motion, produced by ion-ion collisions [27] or by other coupling. The initial radial energy of the ions in the cyclotron motion arises from effects associated with deceleration of the ions in the relatively weak fringe magnetic field above the trap. As the ions approached the trap, the magnetic field became sufficiently strong to guide the ions adiabatically along the field lines, and the effective magnetic moment of the radial orbits became an adiabatic invariant. Estimates of the mean radial energy, based on modeling the deceleration process, indicated that the expected radial energy could be com-

parable to the spread of axial energies of the stored ions, depending on the details of the ion trajectories during deceleration.

Ion-ion collisions tend to equilibrate the ion energies among the degrees of freedom, with a time constant that varies as  $n^{-1}q^{-4}$  at constant mean energy, where  $n$  denotes the ion number density and  $q$  is the charge state [27]. The relatively low density of highly charged ions resulted in an energy equipartition time that was a significant portion of an electron transfer measurement. Transfer of energy between axial and radial degrees of freedom was found to be consistent both with the overall signal changes observed in some of the electron transfer data, and with the estimated ratio of initial axial and radial energies.

It was observed that the linewidths of the ion signals (comparable to the tuned-circuit bandwidth) often tended to increase somewhat during the measurement interval of about 100 s. This cannot be associated with an axial energy decrease, which should produce narrowing, but is compatible with radial diffusion of the stored ions across the lines of magnetic field. Such diffusion might affect the coupling of the ions to the tuned circuit, but this correction was estimated to be negligible, and the linewidth effects were not correlated with the signal changes. The observed sum-signal changes were analyzed based only on collisional energy transfer.

To compensate the data for these signal-changing effects, the sum of the areas of the squared voltage signals with different charges (following corrections for charge state) was fitted to a function of the form  $F(t) = A(1 + B \exp(-t/t_1)) \exp(-t/t_2)$ . The effective time scale for energy transfer is denoted  $t_1$ , and  $t_2$  characterizes the time scale for ion cooling by temporary interaction with the tuned circuit, described above.  $A$  is proportional to the equilibrium axial ion energy, while  $B$  denotes the fraction of axial energy differing from equilibrium. The fitted parameters were  $A$ ,  $B$ ,  $t_1$ , and  $t_2$ . The scaled areas  $S(t)$  for each charge state are then given by the equation  $S(t) = S'(t)/F(t)$  where  $S'(t)$  denotes the measured area at time  $t$ . The time dependences of the scaled data were then proportional only to the time dependences of ion number in each charge state, independent of energy effects. These scaled data were fitted to the solutions of rate equations. Cross sections obtained from analog analysis of the data scaled in this way were compared to cross-section results obtained from digital analysis of the data available for certain measurements taken under the same conditions. The two methods were found to be consistent within the statistical error of 10%, indicating that these corrections to the raw data were adequate. The values of  $B$  obtained from the fits provided information on the (unobserved) relative radial energy of the ions. In the present measurement sequence, initial radial energy was found to exceed initial axial energy only for one charge state studied. Overall, the mean total energy of ions captured in the trap was determined to be about 6 eV in the center-of-mass frame of reference.

The composition and density of the target gas are other important considerations in these measurements. The temperature of the Penning trap and its environs was thermalized at 4.2 K by the large liquid helium reservoir, and no direct density or pressure measurement was feasible. Only  $\text{H}_2$  and He have appreciable vapor pressures at 4.2 K, but they are effectively pumped by the large area of cold surfaces in the

vicinity of the trap. No He was admitted into the vacuum system, but H<sub>2</sub> is a common residual gas in ultrahigh-vacuum systems. A time-of-flight measurement was applied to the products of the charge-exchange reaction between stored Be<sup>2+</sup> ions and the target gas, by a rapid dump of the trapped ions onto the ion detector mounted below the trap. Ions of Be and hydrogen product ions were observed, but no other mass-to-charge ratios. These results provided direct evidence that the target gas was H<sub>2</sub> with negligible impurities. It was noted that after many days at cryogenic temperature, the neutral density at the Penning trap increased, as evidenced by shorter ion storage times associated with increased electron-capture rates. This was interpreted as the effect of H<sub>2</sub> buildup on the cold surfaces raising the local vapor pressure. Following the measurements, it was possible to analyze the residual gas of the vacuum chamber. The partial pressure of H<sub>2</sub> dominated by far, and no residual He was observed.

The density of the target gas was calibrated by performing electron-capture measurements of Ar<sup>11+</sup> with H<sub>2</sub>, in our system. The total cross section for Ar<sup>11+</sup> had been independently measured [11,22]. With the known cross section, mean ion energy, and storage time constant, the H<sub>2</sub> density in the trap was determined, as discussed in Sec. III.

### III. RESULTS AND ANALYSIS

The rate coefficient for electron transfer is usually written as  $k = \int_0^\infty f(v)\sigma(v)v dv$ , where  $f(v)$  is the distribution of relative velocities  $v$  and  $\sigma(v)$  is the cross section. In the present measurements,  $f(v)$  is not well known, but other measurements [11] show that the cross section does not depend significantly on ion velocity. However, the mean ion energy was determined (Sec. II D) so the rate coefficient  $k$  for charge state  $q$  can be approximated as  $k_q = \sigma_q v_{q\text{rms}}$  in terms of an average cross section  $\sigma_q$  and a root mean squared speed determined by the mean energy.

Experimentally, the rate coefficient  $k_q$  was determined using the relation  $k_q = (nT_q)^{-1}$ , where  $T_q$  is the ion storage time constant measured for charge state  $q$  and  $n$  is the H<sub>2</sub> target gas number density determined from the calibration measurements. This density  $n$  was obtained using the relation  $n = (\sigma_s v_{11\text{rms}} T_{11})^{-1}$ .  $T_{11}$  is the time constant for storage of Ar<sup>11+</sup> ions in the target gas of the trap,  $v_{11\text{rms}}$  is their rms velocity, and  $\sigma_s$  is the total cross section for electron transfer from H<sub>2</sub> to Ar<sup>11+</sup> measured at that velocity, using an ion beam technique [11]. However, measurements of single and double electron-transfer collision cross sections of Ar<sup>8+</sup> through Ar<sup>16+</sup> with H<sub>2</sub> have also been completed by Vancura *et al.* [22] in a beam measurement, but at an energy of 2.3  $q$  keV. Although this is well above the energy of present interest, the results of Vancura *et al.* lie close in center-of-mass energy to the upper limit of the energy range studied by Kravis *et al.* [11], in an energy region where the cross section is weakly dependent on energy. The measurements by Vancura *et al.* are distinguished by particular care in the analysis and design of the target gas cell. Their cross sections for single-electron capture have a stated uncertainty of 8%, compared to 10% for the data of Kravis *et al.*, but fall a factor of 2.4 lower for Ar<sup>11+</sup> (i.e., outside the error estimates of both). On the other hand, the measurements of both

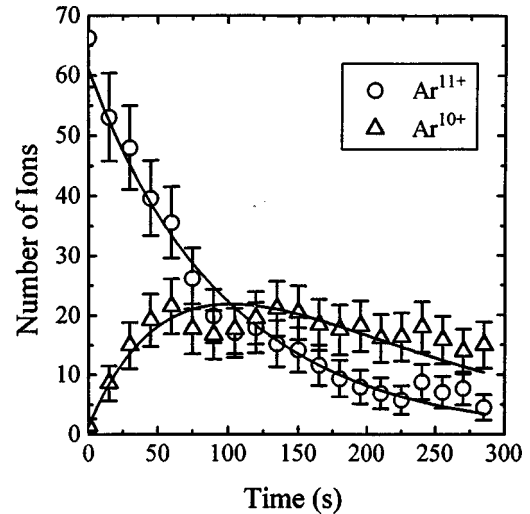


FIG. 5. Storage time constant data were obtained from fits such as these for Ar<sup>11+</sup> ions. With the known storage time constant, plus an adjusted previously published total cross section for this collision, the H<sub>2</sub> target gas density for the highly charged ion collisions was calculated (see Sec. III).

groups agree quite well for charge states 8+ and 9+, and the data of Vancura *et al.* exhibit the expected linear increase with ion charge. The cross sections of Kravis *et al.* double between Ar<sup>9+</sup> and Ar<sup>11+</sup>, after following a general linear increase from Ar<sup>6+</sup> to Ar<sup>9+</sup>. It seems reasonable to scale the Kravis *et al.* results at 6 eV in the center-of-mass frame since their cross sections for Ar<sup>11+</sup> seem anomalously high. The scaling factor  $F = 0.42$  was determined as the ratio of Kravis *et al.* data at their highest energy for Ar<sup>11+</sup> divided by the corresponding data of Vancura *et al.* at their nearby energy. This produces a cross section  $\sigma_s = 1.4 \times 10^{-14}$  cm<sup>2</sup> at 6 eV in the center-of-mass frame. Thus the reference cross section to which the data in Tables I and IV are normalized is  $\sigma_s = F\sigma_{11}$ , where  $\sigma_{11}$  is the sum of single- and double-electron-capture cross sections measured by Kravis *et al.* near 6 eV in the center-of-mass frame. This normalization differs from that originally used in Ref. [20], which was  $\sigma_{11}$ . The data plotted in Fig. 7 now show an improved agreement with the absorbing sphere model, and also agree with the classical over-barrier calculation.

The precision of the measurement of  $T_{11}$  in the ion trap was better than 10%. Representative data for Ar<sup>11+</sup> are shown in Fig. 5. The uncertainties in the fitted total-capture rate and single-capture rate are about 7%. Additionally, there were slow increases in the density  $n$  between calibration points, which influenced repeated measurements of certain rates. During a typical measurement sequence with a given charge state,  $n$  increased by about 20%. Taking this as a conservative measure of uncertainty, and adding independent uncertainties in quadrature, the expected overall accuracy of the determination of  $n$  is about 30%.

Rate equations for the time development of the ion charge states in the trap have been presented in Ref. [20]. The solutions to these rate equations are, for the primary and the secondary charge states,

$$N_0(t) = N_{00} \exp(-\lambda_0 t), \quad (4)$$

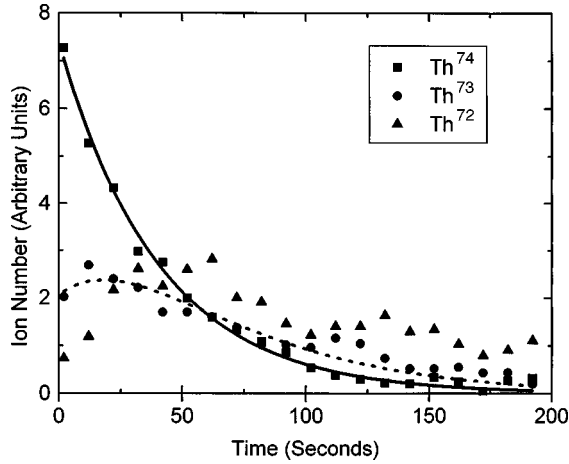


FIG. 6. Fits to the time development of the averaged signals of the  $\text{Th}^{74+}$  and  $\text{Th}^{73+}$  charge states, showing that in this case some  $\text{Th}^{73+}$  was also initially trapped along with the  $\text{Th}^{74+}$  when the measurement was initiated. The  $\text{Th}^{72+}$  data were not fitted in this instance.

$$N_1(t) = N_{00}[\lambda_{0s}/(\lambda_1 - \lambda_0)][\exp(-\lambda_0 t) - \exp(-\lambda_1 t)], \quad (5)$$

where  $N_{00}$  is the initial number of primary ions.  $N_0(t)$  is the number of these ions at time  $t$ , and  $N_1(t)$  is the number of secondary product ions at time  $t$ . The decay rates  $\lambda_0$  and  $\lambda_1$  describe the sum of single and true double capture to the primary and secondary ions, respectively. They can be written in terms of single- and true double-capture rates  $\lambda_{ij}$ , where  $i=0$  or 1 refers to the primary or secondary ion, and  $j=s$  or  $d$  refers to single or true double capture, i.e.,  $\lambda_0 = \lambda_{0s} + \lambda_{0d}$  and  $\lambda_1 = \lambda_{1s} + \lambda_{1d}$ . In certain measurements a small initial population of ions with charge  $q-1$  was observed, due to the injection of ions from an adjacent charge state into the trap. For these measurements,

$$N'_1(t) = N_1(t) + N_{10}\exp(-\lambda_1 t) \quad (6)$$

describes measurements with an initial population  $N_{10}$ . The digital (when possible) and two independent analog analyses were performed on the data. The digital analysis and one of the analog analyses fitted only the first two charge states ( $q$  and  $q-1$ ), while the other analog analysis included additional rate equations to fit peaks down to as far as  $q-4$ . All analyses gave consistent results. Since it was found that the total electron-capture cross sections scaled approximately as  $q$ , the rates  $\lambda_i = (q-i)\lambda_0/q$ , with similar equations for the single- and true double-capture rates, were used for the product ion rates in the analyses. This simplified the fitting procedures for the secondary ions, without biasing the overall data, since  $q$  was high. Figure 6 is a plot of the time evolution of the number of  $\text{Th}^{74+}$ ,  $\text{Th}^{73+}$ , and  $\text{Th}^{72+}$  ions, and the fits to the  $\text{Th}^{74+}$  and  $\text{Th}^{73+}$  data. These fits were used to determine the total reaction rate coefficients  $k_q$  for the primary ions. These rates are presented in Table I. Although there seem to be small variations in rate coefficient between adjacent charge states, the uncertainties in the rate for each charge state are too large to permit definite statements about possible variations in the rates from one charge state to the

TABLE I. Mean total rate coefficients and total cross sections for electron capture from  $\text{H}_2$  to  $\text{Xe}^{q+}$  ions ( $35 \leq q \leq 46$ ) and  $\text{Th}^{q+}$  ions ( $73 \leq q \leq 80$ ), determined relative to the  $\text{Ar}^{11+}$  cross section and then scaled as described in the text. The scaling total cross section  $\sigma_s = 1.4 \times 10^{-14} \text{ cm}^2$ .

Charge state	Total rate coefficient ( $10^{-8} \text{ cm}^3 \text{ s}^{-1}$ )	Total cross section ( $10^{-14} \text{ cm}^2$ )
11+	3.5 (1.1)	1.4 (0.2)
35+	5.5 (3.3)	2.7 (1.1)
43+	8.1 (4.8)	2.9 (1.1)
44+	11.3 (3.6)	4.0 (1.6)
45+	15.2 (5.6)	5.4 (2.1)
46+	8.9 (5.1)	3.1 (1.5)
73+	24.4 (7.5)	10.8 (4.1)
74+	26.1 (8.9)	11.5 (4.4)
75+	28.0 (9.3)	12.3 (4.6)
76+	27.8 (8.9)	12.2 (4.6)
79+	25.0 (7.5)	11.0 (4.2)
80+	25.1 (7.5)	11.1 (4.4)

next. Consequently, average rates were computed over 10% ranges for the Th ions ( $73 \leq q \leq 80$ ) and for the Xe ions ( $43 \leq q \leq 46$ ) [20].

The digital measurements on individual stored Th ion charges were analyzed in terms of the probabilities  $P_n$ ,  $n=0, 1$ , and 2 for the ions making 0, 1, and 2 steps in charge during any measurement interval  $t$ . Assuming the same cross sections for successive charge states, a good approximation for adjacent states at high  $q$ , these probabilities can be written as

$$P_0 = \exp(-\lambda_0 t), \quad (7)$$

$$P_1 = (\lambda_{0s} t) \exp(-\lambda_0 t) = \lambda_{0s} t P_0, \quad (8)$$

$$P_2 = [\lambda_{0d} t + (\lambda_{0s} t)^2 / 2] \exp(-\lambda_0 t) = [\lambda_{0d} t + (\lambda_{0s} t)^2 / 2] P_0. \quad (9)$$

The quadratic term in  $P_2$  accounts for two successive single captures during a measurement interval. The  $P_n$  were experimentally determined by counting the ions in each 5 s interval determined by the measurement ramps. The results for  $P_0$  and  $P_1$  determined  $\lambda_0 = \lambda_{0s} + \lambda_{0d}$  and  $\lambda_{0s}$ . From these rates, the true double-capture rate  $\lambda_{0d}$  was calculated, along with the ratio  $\lambda_{0d}/\lambda_0$ . The mean results for seven measurements on  $\text{Th}^{79+}$  are summarized in Table II. They indicate that the true double-capture fraction  $\lambda_{0d}/\lambda_0 = 0.21(5)$  for this charge state. These results were in agreement with the rates obtained with the fits using the analog analysis method discussed above.

For all data, the averaged, scaled areas for each charge state as a function of time were fitted to Eqs. (4)–(6) to obtain the decay rates  $\lambda_0(q)$  for charge state  $q$ . These rates were then used with the calibrated  $\text{H}_2$  densities to obtain the total cross sections in the form of ratios of rates multiplied by the calibration total cross section, i.e.,  $\sigma_q = \lambda_0(q)/n v_{q\text{rms}} = \sigma_s [\lambda_0(q) v_{11\text{rms}} / \lambda_0(11) v_{q\text{rms}}]$ . Small corrections were also included for the ratio of the root mean squared velocities of the ions, due to the differences in the

TABLE II. Mean probabilities for an ion remaining in the same charge state ( $P_0$ ), for changing one charge state ( $P_1$ ), and for changing two charge states ( $P_2$ ) during 5 s intervals in measurements using digital analysis of individual stored Th<sup>79+</sup> ions. The mean rates for single- ( $\lambda_{0s}$ ), true double- ( $\lambda_{0d}$ ), and total- ( $\lambda_0 = \lambda_{0s} + \lambda_{0d}$ ) electron capture in collisions with H<sub>2</sub> were obtained, and the ratio  $\lambda_{0d}/\lambda_0$  calculated. The results are compatible with those obtained by the analog analysis.

$P_0$	$P_1$	$P_2$	$\lambda_{0s}$	$\lambda_{0d}$	$\lambda_0$	$\lambda_{0d}/\lambda_0$
0.705	0.194	0.076	0.055 (9)	0.0149 (13)	0.0699 (100)	0.213 (50)

distribution of axial and radial velocities for different charge-to-mass ratios, as determined by the data analysis. These total cross sections and the rate coefficients appear in Table I. The true double-to-total capture ratios from the digital analysis of Th<sup>79+</sup> appear in Table II. The mean true double-capture rates relative to the total electron-capture rates, as determined by the fits to the data, appear in Table III. In Table IV, data from Table I were combined for several charge states, for better comparison with the absorbing sphere calculation, including the corrected Ar<sup>11+</sup> data. The uncertainties in the fitted total-capture rate and single-capture rate are about 7% for Ar<sup>11+</sup>. The ratio of the rates for true double-to-total capture is about 9%, in very good agreement with the result of Kravis *et al.* (see Fig. 2 of Ref. [11]), and also with typical results for relative true double capture over a range of Ar charge states [5,22,28,29].

#### IV. DISCUSSION

Due to the low mean collision energies typical of the present measurements, the relatively high charge states, and because of the use of a H<sub>2</sub> target, the most appropriate general theory applicable to these data is the absorbing sphere model of Olson and Salop [1], which is based on Landau-Zener coupling. This theory has been revised in certain cases by reducing the effective coupling [30], but not in the present analysis. Polarization effects in the entrance channel have been added at the suggestion of Olson [31] due to the high ion charge. A unit probability for reaction is assumed to occur below a critical radius  $R_c$  given by the expression [1] in the original analysis

$$R_c^2 \exp[-2.648(2I_t)^{1/2} R_c / q^{1/2}] = 2.864 \times 10^{-4} q(q-1) v_0 / f. \quad (10)$$

The velocity  $v_0 = 5.2 \times 10^{-3}$  a.u. is determined by the mean ion energy, and the first ionization potential  $I_t = 15.4$  eV for H<sub>2</sub> was used. In the recent analysis of low-energy Ar<sup>q+</sup>

TABLE III. Mean results for the ratios of true double-to-total electron-capture rates obtained using fitting procedures to analog data. The mean of all data (digital plus analog analysis) for Th<sup>73-80+</sup> is  $\lambda_{0d}/\lambda_0 = 0.242$  (68). The errors are one standard deviation of the mean of the data.

Charge state $q$	$\lambda_{0d}/\lambda_0$
11+	0.086 (14)
35+	0.205 (25)
(43-45)+	0.263 (32)
(73-80)+	0.267 (93)

+ H<sub>2</sub> collisions [11], the Franck-Condon factor  $f$  was set equal to 1. However, in the initial calculations for H<sub>2</sub> [1], a value of  $f$  much closer to 0.1 was used. The value 0.1 was used in the present calculations.

In collisions of Ar<sup>5+</sup> with D<sub>2</sub>, Giese *et al.* [32] showed that at lower collision energies (500 eV vs 1000 eV in their data), the internuclear separation of D<sub>2</sub> increased, and hence the effective two-electron binding energy decreased, during two-electron-capture collisions. This implies that the usual Franck-Condon calculation will be incorrect for double capture at low energies, but the correct value is unknown. It is assumed here that the 40% error estimate assigned by Olson and Salop to their absorbing sphere calculation [1] includes variations and uncertainties of this type, and that the Franck-Condon factor of 0.1 used in the calculations, although not exact, is adequate within the stated uncertainty. The predicted total cross section is  $\sigma_c = \pi R_c^2$ , which scales approximately as  $q$ , but which yields a lower total cross section at high  $q$  than a strictly linear dependence.

To modify this relation to account for polarization effects, the differences in slopes of the diabatic potential energy curves near  $R_c$  were changed from  $\Delta F = (q-1)/R_c^2$  to  $\Delta F' = [1 - \Gamma(q)](q-1)/R_c^2$ , where  $\Gamma(q) = 2\alpha q/(q-1)R_c^3$  and  $\alpha = 0.8 \times 10^{-24}$  cm<sup>3</sup> is the polarizability of H<sub>2</sub>.  $\Gamma(q)$  was evaluated to first order by inserting the value of  $R_c$  obtained by solving Eq. (10) using the original  $\Delta F$ . Little  $q$  dependence due to polarization was found since  $R_c$  increased with  $q$ . The introduction of the correction  $\Gamma(q)$  had about a 2% effect on the square of the reduced matrix element for the transition, and negligible effect on the predicted total cross section. The accuracy of the absorbing sphere calculation for  $q > 10$  was estimated to be only about 40% in the original work [1].

The absorbing sphere calculation lies below the data in Table IV averaged over  $q$  near  $q = 76$ . However, when the error estimates for the data and for the theory are taken into account, no conclusion about the difference can be drawn.

TABLE IV. Comparison of the mean measured total-electron-capture cross sections with the absorbing sphere prediction. The cross sections are in units of  $10^{-14}$  cm<sup>2</sup>. The absorbing sphere theory is estimated to have an error of about 40% for high charge states.

Charge state	Measured total cross section	Absorbing sphere cross section
11+	1.4 (0.2)	1.6
35+	2.7 (1.1)	3.7
(43-46)+	4.0 (1.4)	4.6
(73-80)+	11.5 (3.8)	6.9

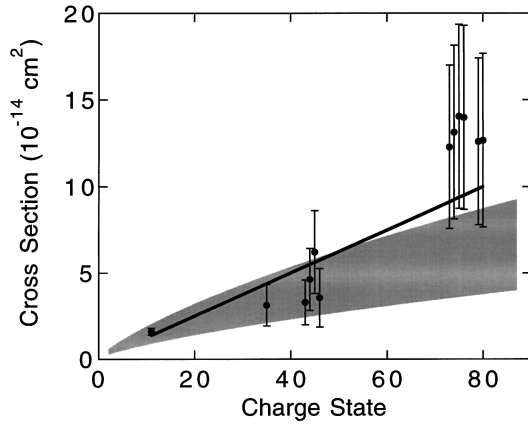


FIG. 7. Total charge-exchange cross sections plotted vs charge state for individual ion measurements (solid circles). The solid line is a fit of the form  $\sigma = aq$  to the data. The shaded region shows the estimated error range for the predicted cross section of the absorbing sphere model. The value and uncertainty for the  $\text{Ar}^{11+}$  data point are from Ref. [11], corrected as described in the text (see Sec. III) by data from Ref. [22].

The prediction of the classical over-barrier model lies between the absorbing sphere prediction and the present data, for  $\text{Th}^{80+}$ . The data overall agree well with a linear dependence of the total cross section on ion charge. Figure 7 is a plot of the total cross-section data for individual charge states vs  $q$ , together with a fit of the form  $\sigma = aq$  to the data and the prediction of the absorbing sphere model.

The relative amount of true double capture to be expected in high- $q$  collisions is still a matter of debate. In the measurements on  $\text{Ar}^{q+} + \text{H}_2$ ,  $6 < q < 11$ , it was found that the true double-capture cross section was less than 10% of the total cross section [11]. True double capture has also been studied for these collision partners in  $\text{Ar}^{q+} + \text{He}$  collisions in higher charge states ( $q = 15 - 18$ ) [5]. It was found for  $\text{Ar}^{16+}$  that true double capture ( $q - 2$  product ions that stabilized radiatively) occurred in “strongly asymmetric” ( $4, n'$ ) states with  $n' > 10$ , while transfer ionization (double capture followed by autoionization resulting in  $q - 1$  product ions) occurred in more symmetric ( $5, n'$ ) states with  $6 \leq n' < 11$ . It was argued that the important quantity in the energy-resonance condition for double-electron transfer is the total binding energy of the two active electrons. Two electrons captured in symmetric states have a higher probability of experiencing an autoionization interaction due to the energy proximity of highly excited  $\text{Xe}^{(q-1)+}$  states [33]. In these measurements [5],  $\sigma_{\text{TI}}/\sigma_{\text{SC}} = 0.13$  near 1.3 keV/ $u$  while Wu *et al.* [29] found  $\sigma_{\text{TI}}/\sigma_{\text{ST}} = 0.24$  at 0.9 keV/ $u$ . Here  $\sigma_{\text{TI}}$  is the cross section for transfer ionization and  $\sigma_{\text{SC}}$  is the single-capture cross section. Both groups found an average probability for radiative stabilization near 9%.

Measurements at much higher charge states on a two-electron target, e.g.,  $\text{Xe}^{q+} + \text{He}$  ( $25 < q < 44$ ) [6] have also been studied at about  $3.4 q$  keV. The data were analyzed in terms of one-electron and two-electron removal from the He target, i.e., true double capture and transfer ionization are both included in two-electron removal. Low observed ratios of the cross sections for these processes were explained by limitations in capture-state densities for the collisions, with no evidence for an increasing importance of transfer-

excitation processes at large  $q$ , which had earlier been suggested as a cause for the low ratios of true double capture.

Data for collisions of  $\text{Xe}^{q+}$  ( $22 < q < 42$ ) with Xe and with He were analyzed in terms of  $P_{\text{rad}} = \sigma_{\text{DC}} / (\sigma_{\text{DC}} + \sigma_{\text{TI}})$  where  $\sigma_{\text{DC}}$  is the cross section for true double capture (radiative stabilization) and  $\sigma_{\text{TI}}$  is the cross section for transfer ionization [4]. Similarities in  $P_{\text{rad}}(q)$  for  $\text{Xe}^{(q-2)+}$  ( $n'l, n'l'$ ) states populated in collisions with Xe and He suggested that the projectile structure, rather than the target structure, was decisive for the balance between transfer ionization and true double capture. A rapid increase from about 0.1 to about 0.4 in  $P_{\text{rad}}(q)$  for  $26 \leq q \leq 36$ , followed by little change with charge for  $36 < q \leq 42$ , for each target, was interpreted in terms of a radiative cascade to the  $4f, n''l''$  states, with subsequent radiative decay (but not autoionization) strongly effected by the number of holes in the  $3d$  shell of  $\text{Xe}^{(q-2)+}$ . The number of  $3d$  holes increases for  $26 \leq q \leq 36$ . Based on this analysis, the next strong increase in  $P_{\text{rad}}(q)$  was then expected only when the  $2p$  shell was opened ( $q \geq 45$ ) for  $\text{Xe}^{q+}$ .

For the case of  $\text{Th}^{q+}$  ions in the present measurements, the  $3d$  shell has many holes, but not the  $2p$  shell, for  $73 \leq q \leq 80$ . Consequently, these ions are analogous to  $\text{Xe}^{q+}$  with  $36 \leq q \leq 45$ , so  $P_{\text{rad}}(q)$  might be expected to have reached a plateau for  $\text{Th}^{q+}$  in this charge range. The plateau value of  $P_{\text{rad}}(q)$  would be expected to be higher, however, since the radiative decay probability relative to that of autoionization is increased by the higher charge of the Th ions. A value of  $P_{\text{rad}} = 0.4$  for  $\text{Xe}^{36+}$  implies  $\sigma_{\text{DC}} = 0.67\sigma_{\text{TI}}$ . Due to the  $q^4$  scaling of the hypothesized  $\Delta n = 1, \Delta l = 1$  transition from the  $4f$  state to a hole in the  $3d$  shell, the radiative stabilization rate might be increased by a factor near 16 for Th ions in our charge range compared to  $\text{Xe}^{36+}$ , leading to  $\sigma_{\text{DC}} \approx 10\sigma_{\text{TI}}$  or  $P_{\text{rad}} \approx 0.9$ . If the mean probability for true double capture is near 0.25, as observed in the present measurements, this implies that autoionization already would contribute only a few percent to the single-capture rate, with little more contribution to be expected for higher charge states, and that true double capture is near its peak value. According to Landau-Zener theory, the maximum probability is one-half that a single electron is captured in traversal in and out through an avoided crossing. If two electrons are captured independently and there is a high probability of radiative stabilization, then true double capture occurs in one-quarter of the collisions. Unfortunately, a direct comparison of our Th data with the published Xe data is not otherwise feasible.

## V. CONCLUSION

Measurements on ions with charge states  $q$  ranging from 35 to 80, produced in EBIT, and recaptured into RETRAP with mean energies less than  $4 q$  eV (6 eV mean collision energy in the center-of-mass frame) have provided results on electron-capture collisions in these charge and energy ranges. Electron capture from  $\text{H}_2$  was studied, to enable a comparison with other measurements at lower charge, and to provide a test of theory. Nondestructive measurement techniques were used, including a technique which enabled the histories of individual highly charged ions to be studied as a function of time, as they changed charge due to collisions with  $\text{H}_2$ .

Because the highly charged product ion numbers were measured, in addition to the primary ion numbers, the ratio of true double-to-total cross sections could be determined.

Analysis of the data showed that the total cross section for electron capture was consistent with a linear dependence on  $q$  in this energy range. The ratio of true double-to-total cross section increased from 9% for Ar<sup>11+</sup> to 20% for Xe<sup>35+</sup>, and remained near 25% for higher  $q$ . The absorbing sphere model predicts comparable values for the total-capture cross section to those measured. Further work is necessary to better understand the electron-transfer process to highly charged high- $Z$  ions.

Additional measurements using this technique with H<sub>2</sub>

targets are feasible with a modified apparatus, which could provide improved precision in results for individual charge states and further comparisons with theory.

#### ACKNOWLEDGMENTS

This research was supported primarily by the U.S. Department of Energy under Contract No. W-7405-ENG-48 with LLNL. Final data analysis and preparation of the manuscript were supported in part by the Robert A. Welch Foundation and the Associated Western Universities (D.A.C.). We thank Ed Magee and Dan Nelson for technical support of these measurements.

- 
- [1] R. E. Olson and A. Salop, *Phys. Rev. A* **14**, 579 (1976).  
 [2] R. Shakeshaft and L. Spruch, *Rev. Mod. Phys.* **51**, 369 (1979).  
 [3] H. Cederquist, H. Andersson, G. Astner, P. Hvelplund, and J. O. P. Pedersen, *Phys. Rev. Lett.* **62**, 1465 (1989).  
 [4] H. Cederquist, H. Andersson, E. Beebe, C. Biedermann, L. Broström, Å. Engström, H. Gao, R. Hutton, J. C. Levin, L. Liljeby, M. Pajek, T. Quinteros, N. Selberg, and P. Sigra, *Phys. Rev. A* **46**, 2592 (1992).  
 [5] H. Cederquist, C. Biedermann, N. Selberg, and P. Hvelplund, *Phys. Rev. A* **51**, 2169 (1995).  
 [6] H. Cederquist, C. Biedermann, N. Selberg, and P. Hvelplund, *Phys. Rev. A* **51**, 2191 (1995).  
 [7] J. B. Delos, *Rev. Mod. Phys.* **53**, 287 (1981).  
 [8] M. S. Huq, C. C. Havener, and R. A. Phaneuf, *Phys. Rev. A* **40**, 1811 (1989).  
 [9] H.-Y. Wang and D. A. Church, *Phys. Rev. A* **36**, 4261 (1987).  
 [10] C. C. Havener, M. S. Huq, H. F. Krause, P. A. Schulz, and R. A. Phaneuf, *Phys. Rev. A* **39**, 1725 (1989).  
 [11] S. Kravis, H. Saitoh, K. Okuno, K. Soejima, M. Kimura, I. Shimamura, Y. Awaya, Y. Kaneko, M. Oura, and N. Shimakura, *Phys. Rev. A* **52**, 1206 (1995).  
 [12] H. Ryufuku, K. Sasaki, and T. Watanabe, *Phys. Rev. A* **2**, 745 (1980).  
 [13] A. Barany, G. Astner, H. Cederquist, H. Danared, S. Huldt, P. Hvelplund, A. Johnson, H. Knudsen, L. Lijeby, and K. G. Rensfelt, *Nucl. Instrum. Methods Phys. Res. B* **9**, 397 (1985).  
 [14] A. Niehaus, *J. Phys. B* **19**, 2925 (1986).  
 [15] L. P. Presnyakov and A. D. Ulantsev, *Kvant Elektron. (Moscow)* **1**, 2377 (1974) [*Sov. J. Quantum Electron.* **4**, 1320 (1975)].  
 [16] R. K. Janev and L. P. Presnyakov, *Phys. Rep.* **70**, 1 (1981).  
 [17] M. A. Levine, R. E. Marrs, J. R. Henderson, D. A. Knapp, and M. B. Schneider, *Phys. Scr.* **T22**, 157 (1988).  
 [18] D. Schneider, D. DeWitt, M. W. Clark, R. Schuch, C. L. Cocke, R. Schmieder, K. J. Reed, M. H. Chen, R. E. Marrs, M. Levine, and R. Fortner, *Phys. Rev. A* **42**, 3889 (1990).  
 [19] D. Schneider, D. A. Church, G. Weinberg, J. Steiger, B. Beck, J. McDonald, E. Magee, and D. Knapp, *Rev. Sci. Instrum.* **65**, 3472 (1994).  
 [20] B. Beck, J. Steiger, G. Weinberg, D. A. Church, J. McDonald, and D. Schneider, *Phys. Rev. Lett.* **77**, 1735 (1996).  
 [21] G. Weinberg, Ph.D. thesis, Texas A&M University, 1995.  
 [22] J. Vancura, V. J. Marchetti, J. J. Perotti, and V. O. Kostroun, *Phys. Rev. A* **47**, 3758 (1993).  
 [23] D. Schneider, M. W. Clark, B. M. Penetrante, J. McDonald, D. DeWitt, and J. N. Bardsley, *Phys. Rev. A* **44**, 3119 (1991).  
 [24] G. Gabrielse, L. Haarsma, and S. L. Rolston, *Int. J. Mass Spectrom. Ion Processes* **88**, 319 (1989).  
 [25] A. Lee, *Rev. Sci. Instrum.* **60**, 3315 (1989).  
 [26] J. Steiger, G. Weinberg, B. Beck, D. A. Church, J. McDonald, and D. Schneider, *Hyperfine Interact.* **108**, 115 (1997).  
 [27] D. A. Church, *Phys. Rev. A* **37**, 277 (1988).  
 [28] C. Biedermann, H. Cederquist, L. R. Andersson, J. C. Levin, R. T. Short, S. B. Elston, J. P. Gibbons, H. Andersson, L. Liljeby, and I. A. Sellin, *Phys. Rev. A* **41**, 5889 (1990).  
 [29] W. Wu, J. P. Giese, I. Ben-Itzhak, C. L. Cocke, P. Richard, M. Stockli, R. Ali, H. Schone, and R. E. Olson, *Phys. Rev. A* **48**, 3617 (1993).  
 [30] K. Taulbjerg, *Z. Phys. D* **21**, S77 (1991).  
 [31] R. E. Olson (private communication).  
 [32] J. P. Giese, C. L. Cocke, W. T. Waggoner, J. O. K. Pedersen, E. Y. Kamber, and L. N. Tunnell, *Phys. Rev. A* **38**, 4494 (1988).  
 [33] J. E. Hansen, *J. Phys. (Paris), Colloq.* **50**, C1-603 (1989).